

## COSMIC RAY SAMPLING OF A CLUMPY INTERSTELLAR MEDIUM

ERIN BOETTCHER<sup>1</sup>, ELLEN G. ZWEIBEL<sup>1,2,3</sup>, TOVA M. YOAST-HULL<sup>2,3</sup>, AND J. S. GALLAGHER III<sup>1</sup>

<sup>1</sup> Department of Astronomy, University of Wisconsin, Madison, WI 53706, USA; boettche@astro.wisc.edu

<sup>2</sup> Department of Physics, University of Wisconsin, Madison, WI 53706, USA

<sup>3</sup> Center for Magnetic Self-Organization in Laboratory and Astrophysical Plasmas, University of Wisconsin-Madison, Madison, WI 53706, USA

Received 2013 September 3; accepted 2013 October 18; published 2013 November 18

### ABSTRACT

How cosmic rays sample the multi-phase interstellar medium (ISM) in starburst galaxies has important implications for many science goals, including evaluating the cosmic ray calorimeter model for these systems, predicting their neutrino fluxes, and modeling their winds. Here, we use Monte Carlo simulations to study cosmic ray sampling of a simple, two-phase ISM under conditions similar to those of the prototypical starburst galaxy M82. The assumption that cosmic rays sample the mean density of the ISM in the starburst region is assessed over a multi-dimensional parameter space where we vary the number of molecular clouds, the galactic wind speed, the extent to which the magnetic field is tangled, and the cosmic ray injection mechanism. We evaluate the ratio of the emissivity from pion production in molecular clouds to the emissivity that would be observed if the cosmic rays sampled the mean density, and seek areas of parameter space where this ratio differs significantly from unity. The assumption that cosmic rays sample the mean density holds over much of parameter space; however, this assumption begins to break down for high cloud density, injection close to the clouds, and a very tangled magnetic field. We conclude by evaluating the extent to which our simulated starburst region behaves as a proton calorimeter and constructing the time-dependent spectrum of a burst of cosmic rays.

*Key words:* cosmic rays – galaxies: individual (M82) – galaxies: ISM – galaxies: starburst

*Online-only material:* color figures

### 1. INTRODUCTION

Starburst galaxies are complex environments with intense star formation, “clumpy,” multi-phase interstellar gas, supernovae-driven winds, and tangled magnetic fields. It is remarkable, then, that despite drastically different environments, both quiescent and star-forming disk galaxies have a well-established linear correlation between their far-infrared (FIR) and radio luminosities (Helou et al. 1985). In these systems, the FIR–radio luminosity correlation suggests a fundamental relationship between the star formation processes, resulting in FIR emission from dust heated by young, massive stars, and the cosmic ray population, producing radio synchrotron emission from relativistic electrons spiraling along magnetic field lines.

To explain the FIR–radio luminosity correlation, the cosmic ray calorimeter model for starburst galaxies has been explored (e.g., Voelk 1989; Thompson et al. 2006; Persic et al. 2008; de Cea del Pozo et al. 2009; Lacki et al. 2011; Paglione & Abrahams 2012; Yoast-Hull et al. 2013). This model suggests that the energy imparted to cosmic rays by supernovae is entirely expended through observable emission within the starburst region. If this model holds for cosmic ray electrons, then the observed radio synchrotron emission should be solely dependent on the supernova rate and therefore on the star formation rate (SFR; there is, of course, also a dependence on magnetic field strength, but this too appears to be tied to the SFR; Schleicher & Beck 2013). Likewise, if the model holds for cosmic ray protons, then we expect a similar relationship between the observed  $\gamma$ -ray emission from pion production and the SFR.

In order to test the calorimeter model for starburst galaxies, it is necessary to understand how cosmic rays sample the multi-phase interstellar medium (ISM) as they undergo radiative, collisional, and advective losses within the starburst region. In an ISM consisting of cold, molecular clouds embedded

in a hot, low-density medium, cosmic rays will only sample the mean density of the ISM if they are able to effectively enter the molecular clouds. The leading theory of cosmic ray acceleration suggests that energetic particles undergo first-order Fermi acceleration (Fermi 1949), or diffusive shock acceleration (e.g., Bell 1978; Blandford & Ostriker 1978), at supernova shock fronts. Additionally, cosmic rays may undergo second-order Fermi acceleration (Fermi 1949) in the diffuse ISM. Both first- and second-order Fermi acceleration can only occur efficiently in low-density environments, where the acceleration mechanism can impart energies in excess of ionization losses and the small-scale magnetic field fluctuations which scatter the particles can propagate. For these reasons, the majority of cosmic rays are believed to be injected in the hot, low-density medium.

The hot medium where cosmic rays are injected has a very large filling factor compared to the molecular gas. Additionally, the hot medium may be actively advected from the region by a galactic wind. In order for the cosmic rays to sample the mean density of the ISM, the magnetic field lines along which they propagate must intersect a sufficiently large number of molecular clouds, and the cosmic rays must remain within the region for a sufficiently long time before they are advected away. Therefore, cosmic ray sampling of the mean density of the ISM is far from a foregone conclusion.

In this paper, we use Monte Carlo simulations to study cosmic ray sampling of an ISM with properties similar to that of the prototypical starburst galaxy M82. We selected this galaxy for our study because it has a well-studied starburst region with well-observed masses of its multi-phase ISM, galactic wind speed, and supernova rate. In M82, the ISM consists of a hot, diffuse medium in which dense, warm, ionized gas and dense, cold, molecular clouds are found (e.g., Westmoquette et al. 2009). In particular, CO measurements suggest that the galaxy contains  $\sim 3 \pm 1 \times 10^8 M_{\odot}$  of molecular gas that is largely

**Table 1**  
Properties of M82

Physical Parameters	Values	References
Distance	3.9 Mpc	1
Radius SB	200 pc	2
Scale height SB	100 pc	2
Molecular gas mass	$\sim 3 \pm 1 \times 10^8 M_\odot$	3, 4
Wind speed (optical)	$\sim 500\text{--}600 \text{ km s}^{-1}$	5
Wind speed (X-ray)	$\sim 1400\text{--}2200 \text{ km s}^{-1}$	6

**References.** (1) Sakai & Madore 1999; (2) Förster Schreiber et al. 2003; (3) Naylor et al. 2010; (4) Wild et al. 1992; (5) Shopbell & Bland-Hawthorn 1998; (6) Strickland & Heckman 2009.

found within clumpy clouds in the starburst region (e.g., Naylor et al. 2010). Additionally, M82 has a well-observed galactic wind that travels approximately perpendicularly to the galactic plane and is believed to be primarily driven by supernova shock heating (Chevalier & Clegg 1985). Estimates of the outflow velocity range from  $\sim 500\text{--}600 \text{ km s}^{-1}$  as indicated by optical emission lines of ionized gas (Shopbell & Bland-Hawthorn 1998, and references therein) to as high as  $\sim 1400\text{--}2200 \text{ km s}^{-1}$  as suggested by X-ray observations (Strickland & Heckman 2009). Although we use properties suggestive of M82 in this study (see Table 1 for a summary), our analysis is applicable to many other such systems.

Here, we evaluate how cosmic ray sampling of the ISM in starburst galaxies is affected by the number of molecular clouds, the galactic wind speed, the extent to which the magnetic field is tangled, and the cosmic ray injection mechanism. In Section 2, we describe our Monte Carlo simulation parameters and the calculation of an emissivity ratio used to quantify the sampling behavior of the cosmic ray population. Section 3 details the results of our simulations and highlights the region of parameter space in which the emissivity ratio is elevated by a factor of a few. In Section 4, we review our results, compare them to existing models, and discuss their implications for exploring the cosmic ray calorimeter model and constructing the time-dependent spectrum of a burst of cosmic rays.

## 2. MONTE CARLO SIMULATIONS

### 2.1. Simulation Parameters

The multi-phase ISM in the starburst region is modeled to consist of a hot, low-density medium in which cold molecular clouds are embedded. Observations and numerical simulations suggest that the molecular medium consists of many clumpy, fragmented clouds (e.g., Blitz 1993; Inoue & Inutsuka 2012). Although  $\sim 3 \pm 1 \times 10^8 M_\odot$  of molecular gas has been detected in the starburst nucleus (e.g., Naylor et al. 2010), we take a conservative order of magnitude estimate of  $\sim 1 \times 10^8 M_\odot$  of molecular gas within our spherical starburst region of radius  $R = 100 \text{ pc}$ , corresponding to a mean number density  $\langle n \rangle \sim 486 \text{ cm}^{-3}$ . Assuming that the upper limit on the maximum mass of giant molecular clouds in the Milky Way of  $\sim 10^4\text{--}10^6 M_\odot$  is applicable to M82, this implies on the order of  $N_c \sim 10^3$  molecular clouds. We hold the total mass of molecular gas constant while varying the number of clouds from  $N_c = 200$  to  $N_c = 3000$  clouds to explore both the nominal case ( $N_c \sim 3000$ ) as well as the limit of very small cloud numbers and very high cloud densities ( $N_c \sim 200$ ). Each cloud is taken to have a volume of  $V_c \sim 27 \text{ pc}^3$ , and thus the clouds' volume filling factor varies from  $\sim 0.1\%$  to  $\sim 2\%$ .

Note that we are explicitly neglecting the contribution of the hot, low-density medium to the density sampled by cosmic rays. Due to the diffusive nature of particle motion along magnetic field lines (which reduces their effective propagation speed from  $c$  to the Alfvén speed,  $v_A$ ), the contribution of the low-density gas is greater than the simple ratio  $\langle n_h \rangle / \langle n_c \rangle$ , where  $\langle n_h \rangle$  and  $\langle n_c \rangle$  are the mean densities of the hot gas and the cold molecular gas, respectively. We estimate that this is approximately a 10% effect for the M82 environment. Likewise, warm ( $\sim 10^4 \text{ K}$ ) ionized gas, in addition to hot gas and cold molecular gas, is undoubtedly present and would also have a small effect on the model. We will consider these small contributions in future work.

Additionally, a supernova-driven galactic wind is included in the model with a linear profile and a wind speed of  $v_{\text{adv}}$  at a height  $z = 100 \text{ pc}$  above the midplane ( $v = v_{\text{adv}}(z/100 \text{ pc})$ ). We vary  $v_{\text{adv}}$  from 0 to  $2000 \text{ km s}^{-1}$ , with  $500 \text{ km s}^{-1}$  nominally taken as the favored value (Yoast-Hull et al. 2013). We assume the wind carries away the magnetic field lines embedded in the hot gas, together with the cosmic rays loaded onto the field lines, but that the molecular component remains behind.

Since the starburst region of M82 is highly turbulent, we expect the magnetic field to have a significant random component. Cosmic ray propagation along tangled magnetic field lines is approximated as a random walk process governed by a mean free path,  $\lambda_{\text{mfp}}$ , which parameterizes the magnetic correlation length. As the magnetic geometry is not well known, we vary  $\lambda_{\text{mfp}}$  from 0.5 pc to 25 pc. A longer value of  $\lambda_{\text{mfp}}$  (i.e.,  $\lambda_{\text{mfp}} = 50 \text{ pc}$ ) was found to yield comparable results to the  $\lambda_{\text{mfp}} = 25 \text{ pc}$  case. Due to scattering by short wavelength Alfvén waves generated by the cosmic ray streaming instability, cosmic rays are taken to travel along the field lines at the Alfvén speed,  $v_A$  (Kulsrud & Pearce 1969). Given a magnetic field strength  $B = 275 \mu\text{G}$  and an average density of the hot medium  $\langle n \rangle = 0.33 \text{ cm}^{-3}$  (Yoast-Hull et al. 2013), the Alfvén speed is found to be  $v_A = 960 \text{ km s}^{-1}$ .

We use three methods of injecting the cosmic rays into the starburst region. First, we consider the simple scenario where all cosmic rays are injected at the center of the region. Second, in accordance with models of distributed cosmic ray acceleration such as second-order Fermi acceleration by interstellar turbulence, we inject the particles randomly throughout the region. Finally, in agreement with models of point source cosmic ray acceleration such as first-order Fermi acceleration by supernova shocks, we inject the particles at randomly chosen supernova shock sites. We choose 30 injection sites due to observational evidence from radio interferometry for  $\sim 30$  active supernova remnants (SNRs) in M82 (e.g., Fenech et al. 2010). One might expect SNRs and star-forming molecular clouds to spatially coincide, as young, massive stars are not likely to travel far from their place of birth over the course of their lifetimes. Additionally, recent observations of  $\gamma$ -ray emission from molecular clouds associated with SNRs (e.g., Aharonian et al. 2008a, 2008b; Abdo et al. 2010, 2011; Ajello et al. 2012) provide evidence for a spatial correlation between SNRs and molecular clouds. Thus, for our final injection method, our injection sites are chosen randomly on spheres of radius  $r = 3 \text{ pc}$  centered on clouds. For all cosmic ray injection methods, we disallow injection inside of clouds due to the reduced acceleration efficiency expected in cold, dense environments.

The Monte Carlo simulations are run with  $N_p = 10^4$  particles for a given choice of  $N_c$ ,  $v_{\text{adv}}$ ,  $\lambda_{\text{mfp}}$ , and cosmic ray injection mechanism (see the Appendix for a discussion of the number of particles necessary to achieve convergence). At the beginning

**Table 2**  
Model Parameters

Parameters	Values
Geometry of SB	Spherical
Radius of SB	100 pc
Molecular gas mass	$1 \times 10^8 M_{\odot}$
Mean ISM density $\langle n \rangle^a$	$486 \text{ cm}^{-3}$
Number of clouds $N_c$	200–3000
Mean free path $\lambda_{\text{mfp}}$	0.5–25 pc
Alfvén speed $v_A$	$960 \text{ km s}^{-1}$
Wind speed $v_{\text{adv}}$	0–2000 $\text{km s}^{-1}$

**Note.** <sup>a</sup> Derived from above parameters for an average particle mass of twice the proton mass.

of a run, we select the cosmic rays’ initial injection sites as well as a random molecular cloud distribution, and we map the state of the ISM onto a three-dimensional grid with a resolution of 0.5 pc. Starting from its injection site, a given particle executes a random walk governed by a mean free path  $\lambda_{\text{mfp}}$  broken down into steps of length  $l = 0.5$  pc. At each step, the contribution of advection to the particle motion, the component of the ISM being sampled (in/out of cloud), and the particle’s presence in the starburst region (in/out of region) are assessed. If a particle is inside of a cloud at the beginning of a step, the galactic wind does not act on the particle for that step, and the particle is taken to travel at the speed of light instead of at the Alfvén speed. The particles are taken to free-stream inside of molecular clouds due to the destruction by ion–neutral damping of Alfvén waves resulting from the streaming instability (Kulsrud & Pearce 1969). The particle is scattered when it has traveled a distance equal to its mean free path, and the process repeats until the particle has traveled out of the region.

Note that we do not explicitly model energy losses along the particle trajectories, deferring a discussion of it to Section 4. The cloud column densities ( $\sim 5 \times 10^{23} \text{ cm}^{-2}$ ,  $N_c = 3000$  clouds;  $\sim 7 \times 10^{24} \text{ cm}^{-2}$ ,  $N_c = 200$  clouds) are well below the characteristic column densities for energy loss ( $N_E \sim 2 \times 10^{26} \text{ cm}^{-2}$ ,  $E = 1 \text{ GeV}$ ;  $N_E \sim 3 \times 10^{25} \text{ cm}^{-2}$ ,  $E = 1 \text{ TeV}$ ) except for very small  $N_c$  and/or very high proton energies. This suggests that cosmic rays make several passes through clouds before undergoing collisional energy losses. See Table 2 for a summary of our model parameters.

Figure 1 summarizes the sampling behavior of the cosmic rays for a single representative run of the Monte Carlo code. For each  $\lambda_{\text{mfp}}$ , we show distributions of the total distance traveled, the total distance traveled in molecular clouds, and the average density sampled ( $\langle \rho_P \rangle$ ) normalized to the mean density of the ISM in the starburst region ( $\langle \rho_{\text{SB}} \rangle$ ). It is clear from the density distributions that the particles display a diverse range of sampling behaviors. The extremes of this behavior are seen in the peaks at  $\langle \rho_P \rangle / \langle \rho_{\text{SB}} \rangle = 0$ , where no clouds are sampled, as well as in the tails at  $\langle \rho_P \rangle / \langle \rho_{\text{SB}} \rangle \gtrsim 5$ , where the particles sample densities as high as an order of magnitude greater than the mean density of the ISM. Note that for  $\lambda_{\text{mfp}} > 1$ , a peak appears near  $\langle \rho_P \rangle / \langle \rho_{\text{SB}} \rangle = 1$ . These trends hint that as we proceed to more precisely quantify the sampling behavior, we may reasonably expect the particles to roughly sample the mean density of the ISM over much of parameter space.

## 2.2. Emissivity Calculations

To quantitatively assess the assumption that cosmic rays sample the mean density of the ISM in the starburst region

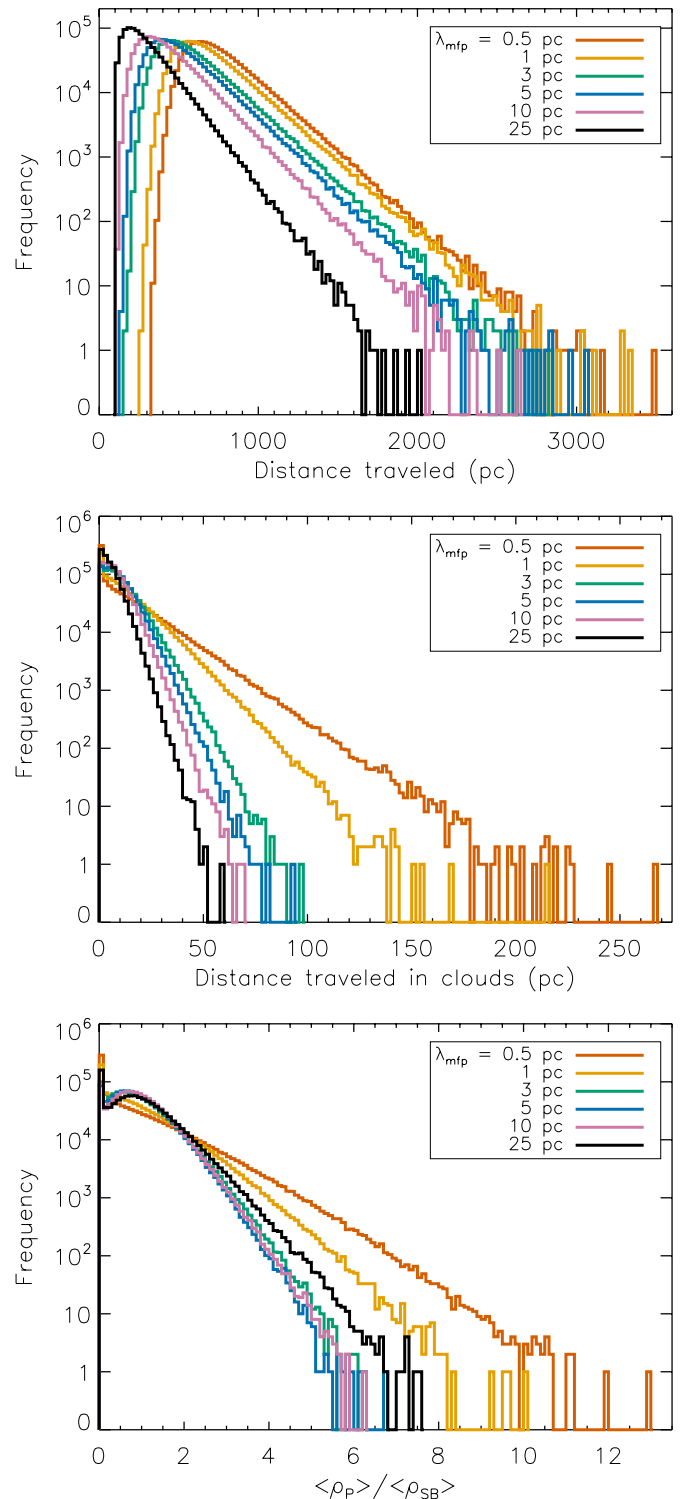


**Figure 1.** Summary of the cosmic ray sampling behavior during a representative run of the Monte Carlo code for each  $\lambda_{\text{mfp}}$  considered. From top to bottom, the figures show the distance traveled by particles before leaving the starburst region, the distance traveled inside of molecular clouds, and the average density sampled normalized to the mean density of the ISM, neglecting any contribution from the hot or warm ionized gas. The particles show a significant range of sampling behaviors; all density distributions show a peak at  $\langle \rho_P \rangle / \langle \rho_{\text{SB}} \rangle = 0$ , where the particles sample no clouds, as well as varying degrees of a tail at  $\langle \rho_P \rangle / \langle \rho_{\text{SB}} \rangle \gtrsim 5$ , where they sample average densities greater than the mean density of the ISM by as much as an order of magnitude. These results were found for injection at the center of the starburst region,  $N_c = 3000$  clouds,  $v_{\text{adv}} = 500 \text{ km s}^{-1}$ , and  $N_p = 10^6$  particles, although the results are broadly consistent with the full parameter space.

(A color version of this figure is available in the online journal.)

and evaluate its effect on  $\gamma$ -ray emission, we use our simulation results to construct a function  $\varphi(n/\langle n \rangle)d(n/\langle n \rangle)$ , which gives the fraction of cosmic rays that sample gas density  $n$  relative to the mean density  $\langle n \rangle$ . The emissivity due to pion production by cosmic rays in molecular clouds is then given by

$$\epsilon = \int \varphi\left(\frac{n}{\langle n \rangle}\right) n_{\text{cr}} n \langle \sigma_{\text{coll}} v \rangle E_{\text{int}} d\left(\frac{n}{\langle n \rangle}\right), \quad (1)$$

where  $n$  and  $n_{\text{cr}}$  are the number densities of the medium and the cosmic rays, respectively,  $\sigma_{\text{coll}}$  is the cross section for pion production,  $v$  is the velocity of the particles, and  $E_{\text{int}}$  is the energy produced by the interaction. If the cosmic rays do indeed sample the mean density of the ISM, the emissivity is given by

$$\epsilon_0 = n_{\text{cr}} \langle n \rangle \langle \sigma_{\text{coll}} v \rangle E_{\text{int}}. \quad (2)$$

Thus, the ratio of emissivities  $\alpha$  is given by

$$\alpha = \frac{\epsilon}{\epsilon_0} = \int \varphi\left(\frac{n}{\langle n \rangle}\right) \left(\frac{n}{\langle n \rangle}\right) d\left(\frac{n}{\langle n \rangle}\right). \quad (3)$$

Although  $\sigma_{\text{coll}}$  is a function of energy,  $\alpha$  is independent of energy for all cosmic rays that satisfy the propagation assumptions given at the beginning of this section (i.e., the streaming instability results in propagation at the Alfvén speed).  $\alpha$  is easily obtained by appropriately normalizing, binning, and summing over the distributions of average densities sampled weighted by the densities themselves (see, e.g., Figure 1(c)). Thus, we determine  $\alpha$  for the range of parameters discussed in Section 2.1 and seek areas of parameter space where  $\alpha$  departs significantly from unity. See the Appendix for a discussion of our determination of  $\alpha$  for a given choice of  $N_c$ ,  $v_{\text{adv}}$ ,  $\lambda_{\text{mfp}}$ , and cosmic ray injection mechanism. The Appendix also details our estimation of the errors on  $\alpha$  that originate from both the finite number of particles per run as well as the changes in the random cloud distributions and injection sites from run to run.

### 3. RESULTS

#### 3.1. Emissivity Ratios for all Parameters

We begin by examining the densities sampled over the entire range of parameters considered in this study (i.e., all combinations of cosmic ray mean free path, injection mechanism, two molecular cloud numbers ( $N_c = 200, 3000$  clouds), and three wind speeds ( $v_{\text{adv}} = 0, 500, \text{ and } 2000 \text{ km s}^{-1}$ )). In Figure 2, we see that the cosmic rays roughly sample the mean density of the ISM over much of parameter space. Overall, we do not achieve emissivities suppressed below  $\alpha = 1$  by a factor of more than  $\sim 2$ ; we do achieve emissivities elevated above  $\alpha = 1$  by a factor of a few; and these modestly elevated emissivities occur only for cosmic ray injection near clouds in the limit of small cloud number and thus high cloud density. This case will be considered separately in Section 3.2.

Although  $0.5 \lesssim \alpha \lesssim 1.8$  over much of parameter space, there are still clear trends relating  $\alpha$  to  $N_c$ ,  $\lambda_{\text{mfp}}$ ,  $v_{\text{adv}}$ , and cosmic ray injection mechanism. We note that  $\alpha$  tends to increase as  $\lambda_{\text{mfp}}$  decreases, suggesting that cosmic rays with short  $\lambda_{\text{mfp}}$  generally travel along more convoluted trajectories and thus spend more time sampling the starburst region as well as the clouds that they encounter. We also note a somewhat greater spread in  $\alpha$  at shorter  $\lambda_{\text{mfp}}$  that may be due to more frequent scattering allowing for more varied paths through the starburst region and thus more varied emissivity outcomes.

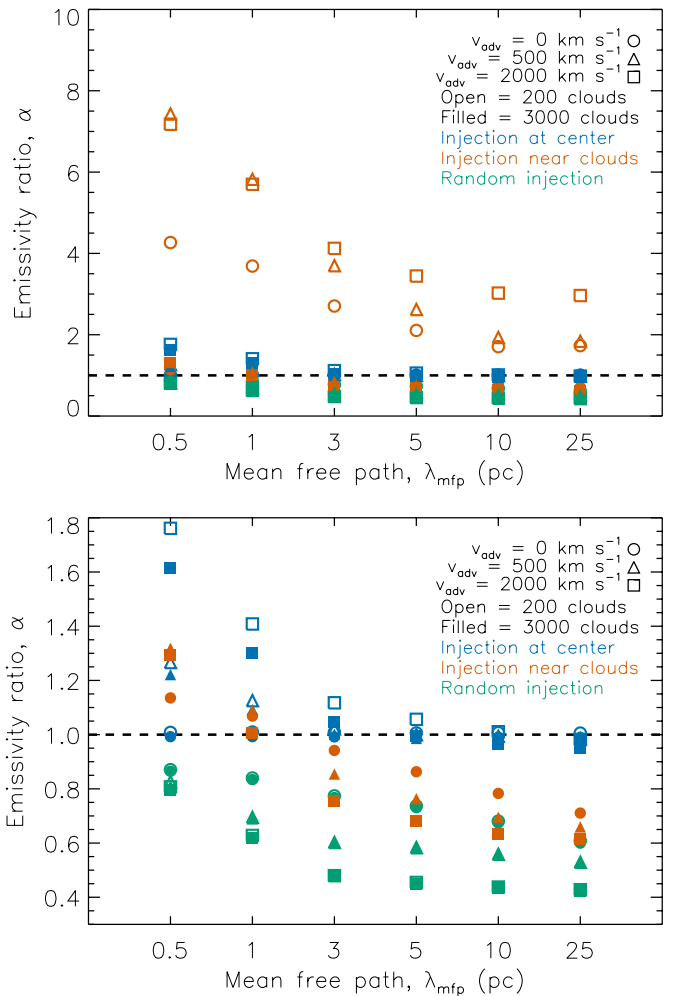


**Figure 2.** Mean emissivities for all combinations of cosmic ray mean free path, injection mechanism (indicated by color), three wind speeds (shape), and two cloud numbers (fill). The lower panel is a closer view of a portion of the upper. It is clear that over the vast majority of parameter space, the emissivity ratios are clustered around  $\alpha = 1$  and thus the cosmic rays roughly sample the mean density of the ISM. However, as discussed in Section 3.2, cosmic ray injection near the clouds in the limit of small cloud number and thus high cloud density results in emissivity ratios that are elevated by a factor of a few and the assumption that the cosmic rays sample the mean density breaks down. Additionally, cosmic ray injection randomly throughout the region results in emissivities that are suppressed by as much as a factor of  $\sim 2$ ; however, the suppression of the emissivity at low values of  $\alpha$  is not as dramatic as its elevation at high  $\alpha$ .

(A color version of this figure is available in the online journal.)

For cosmic ray injection near clouds and randomly throughout the region,  $\alpha$  tends to decrease as  $v_{\text{adv}}$  increases. When injection occurs far from the midplane, the particle's trajectory is immediately affected by the wind, and advective losses dominate. However, for injection at the center of the region and short  $\lambda_{\text{mfp}}$ ,  $\alpha$  instead increases with  $v_{\text{adv}}$ . For central injection, the particle initially experiences very weak wind speeds, and advective losses are negligible. Additionally, for higher  $v_{\text{adv}}$ , these particles may travel along more efficient trajectories and thus sample more clouds than for lower  $v_{\text{adv}}$ , where they travel more convoluted trajectories and are more likely to circumvent clouds.

The cosmic ray injection mechanism also has other effects on the value of  $\alpha$ . At a given  $\lambda_{\text{mfp}}$ , emissivities from injection at the center of the starburst region exceed those of injection randomly

throughout the region, while injection near clouds in the case of  $N_c = 3000$  clouds tends to fall between these two limiting cases. It is expected that cosmic rays injected at the center have the opportunity to sample greater densities than those injected randomly because they generally spend more time within the starburst region. Additionally, cosmic rays injected near clouds in the  $N_c = 3000$  clouds case are expected to sample greater densities than those injected randomly because of their initial proximity to clouds. However, as these cosmic rays also sample lesser densities than those injected at the center of the region, it appears that this effect is outweighed by the relatively shorter time spent within the region.

Finally,  $N_c$  has a clear effect on the value of  $\alpha$ , albeit one moderated by injection mechanism. When cosmic rays are injected near clouds and thus have ample opportunity to encounter dense gas, a smaller number of denser clouds produces a higher emissivity than a larger number of less dense clouds. However, when cosmic rays are randomly injected, they have a decreased likelihood of encountering dense gas; thus, despite the increase in cloud density, the decrease in cloud number may suppress the emissivity such that the results are comparable for both a low and high number of clouds.

### 3.2. Emissivity Ratios for Injection Near $N_c = 200$ Clouds

We now discuss the region of parameter space where the cosmic rays sample the highest  $\alpha$  values ( $2 \lesssim \alpha \lesssim 7.5$ ) when injected near the molecular clouds in the limit of small cloud number ( $N_c = 200$  clouds) and thus high cloud density. This result is not surprising, as cosmic ray injection near high-density molecular gas has the greatest likelihood of interaction between the particles and the molecular medium. As noted in Section 3.1, the value of  $\alpha$  is highest for short  $\lambda_{\text{mfp}}$  ( $\lambda_{\text{mfp}} \lesssim 5$  pc), where  $\alpha$  varies from  $\sim 2$ – $7.5$ , than for longer  $\lambda_{\text{mfp}}$ , where  $\alpha$  is  $\sim 2$ – $3$ . In addition to spending more time sampling the starburst region, particles with short  $\lambda_{\text{mfp}}$  may also be more likely to enter the clouds accompanying their injection sites than those that are able to travel more efficiently away.

As is clear in Figure 3, the case of no galactic wind results in  $\alpha$  values lower than that of high wind ( $v_{\text{adv}} = 2000$  km s $^{-1}$ ) by a factor of  $\sim 2$ , while the case of moderate wind ( $v_{\text{adv}} = 500$  km s $^{-1}$ ) results in intermediate emissivities. At short  $\lambda_{\text{mfp}}$ , the cases of high and moderate  $v_{\text{adv}}$  become comparable. Particles that are injected between the galactic plane and their accompanying cloud are likely to be advected into the cloud in the presence of a wind; the likelihood of this occurring may increase with  $v_{\text{adv}}$ . Particles with short  $\lambda_{\text{mfp}}$  also have an increased likelihood of entering the clouds at their injection sites due to their inability to efficiently travel away from these sites, rendering the emissivity less sensitive to  $v_{\text{adv}}$ .

In summary, cosmic ray injection near  $N_c = 200$  clouds for short  $\lambda_{\text{mfp}}$  and moderate to high  $v_{\text{adv}}$  results in  $\alpha$  values that are modestly elevated above  $\alpha = 1$  by a factor of a few. Note that the uncertainty associated with these emissivities increases dramatically in the limit of short  $\lambda_{\text{mfp}}$  and high  $v_{\text{adv}}$ . The former dependence suggests that particles that experience more frequent scattering travel along more diverse trajectories and thus have more diverse emissivity outcomes. Additionally, the latter dependence implies that a higher  $v_{\text{adv}}$  results in greater populations of particles that are rapidly advected away (resulting in low emissivities) as well as particles that enter the clouds near their injection sites (high emissivities). Therefore, although this region of parameter space results in elevated emissivities, the

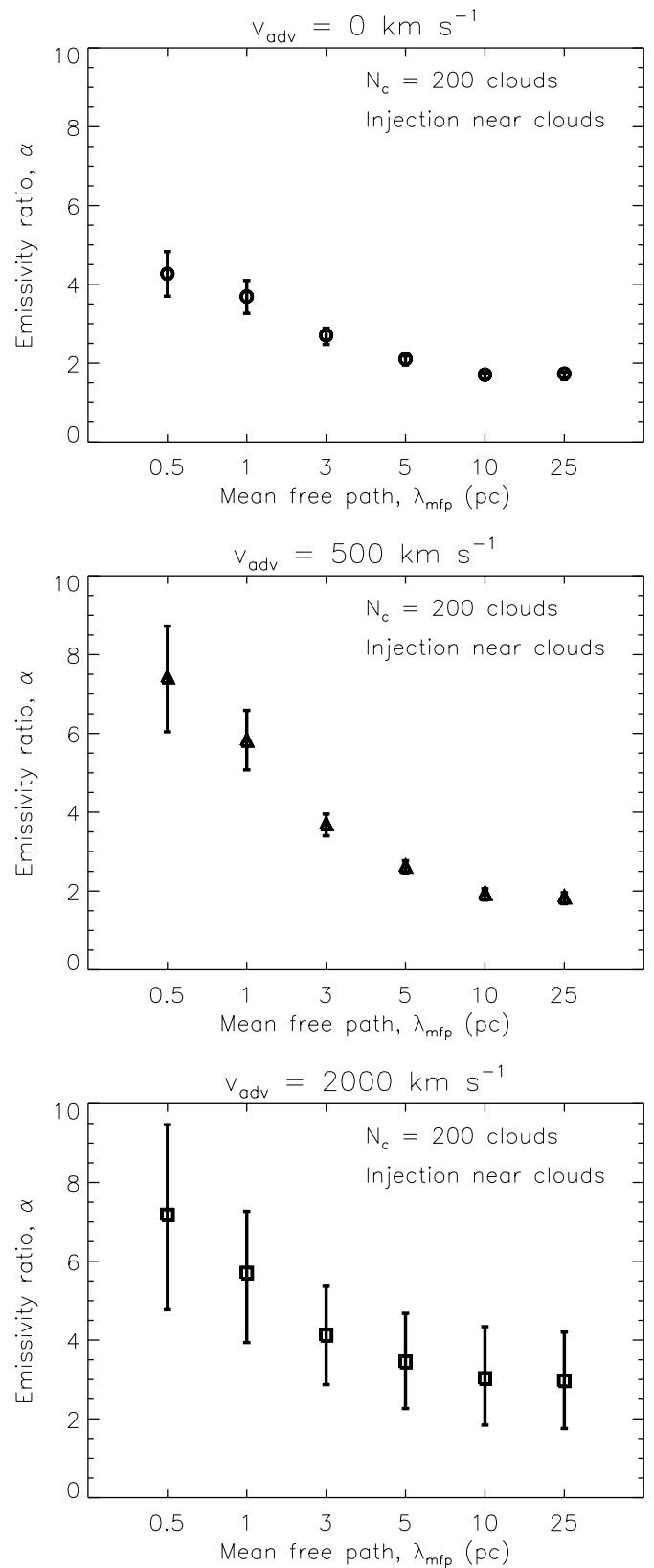


**Figure 3.** Mean emissivities and 68% confidence intervals for cosmic ray injection near clouds in the limit of small cloud number ( $N_c = 200$  clouds) and high cloud density. In this region of parameter space, we achieve emissivities elevated above  $\alpha = 1$  by a factor of a few, with the highest emissivities achieved with large  $v_{\text{adv}}$  and small  $\lambda_{\text{mfp}}$ .

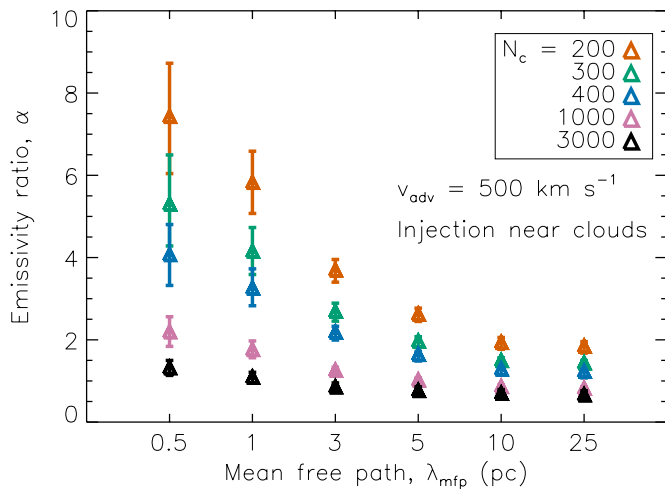


**Figure 4.** Mean emissivities and 68% confidence intervals are strongly dependent on the cloud number and thus the cloud density for cosmic ray injection near clouds. Though the emissivity is significantly elevated for short  $\lambda_{\text{mfp}}$  in the limit of small  $N_c$ , these emissivities decrease very rapidly as  $N_c$  increases. At  $N_c$  values greater than several hundred,  $\alpha$  approaches unity for all  $\lambda_{\text{mfp}}$ . (A color version of this figure is available in the online journal.)

nature of the random cloud and injection point distributions is important in determining the observed emissivity.

We have now seen that cosmic rays injected near  $N_c = 200$  high-density clouds sample densities in excess of the mean density of the ISM, while those injected near  $N_c = 3000$  lower density clouds do not. Thus, for the case of injection near clouds, we seek an upper limit on the number of clouds necessary to achieve elevated emissivities. In Figure 4, we consider  $\alpha$  for  $v_{\text{adv}} = 500 \text{ km s}^{-1}$  and a range of  $N_c$  values for which  $200 \leq N_c \leq 3000$  clouds. It is clear that very low values of  $N_c$  are required to achieve elevated emissivities. For the shortest  $\lambda_{\text{mfp}}$ , decreasing  $N_c$  from 3000 to 1000 clouds increases  $\alpha$  by only a factor of  $\sim 2$ . It is only when  $N_c$  is decreased to  $\sim 400$  clouds that  $\alpha$  becomes elevated by a factor of a few. Thus, in the case of cosmic ray injection near clouds, a very small cloud number and thus very high cloud density is required to achieve elevated emissivities.

### 3.3. Cosmic Rays that Do Not Sample Clouds

We now consider the fraction of cosmic rays that escape from the starburst region without sampling molecular clouds at all. This sheds light on the relationship between the sampling behavior of individual particles and the sampling of the particle population as a whole. In Figure 5, it is clear that over the full parameter space considered, the fraction  $f$  of cosmic rays that escape from the starburst region without sampling clouds ranges from near complete sampling ( $f \sim 2 \times 10^{-5}$ ,  $N_c = 3000$  clouds,  $v_{\text{adv}} = 0 \text{ km s}^{-1}$ , injection at the center) to near complete escape ( $f \sim 0.98$ ,  $N_c = 200$ ,  $v_{\text{adv}} = 2000 \text{ km s}^{-1}$ , random injection). As we found that cosmic rays approximately sample the mean density of the ISM over much of parameter space, we see that emissivity values of  $\alpha \sim 1$  are achieved over the full range in  $f$ . Therefore, we may find  $\alpha \sim 1$  both when the vast majority of particles sample roughly the mean density (occurring mainly for high  $N_c$  values), as well as when only a small minority of particles encounter the molecular medium (mainly low  $N_c$  values).

When we are interested in the mean density sampled by the cosmic ray population as a whole, such as when evaluating

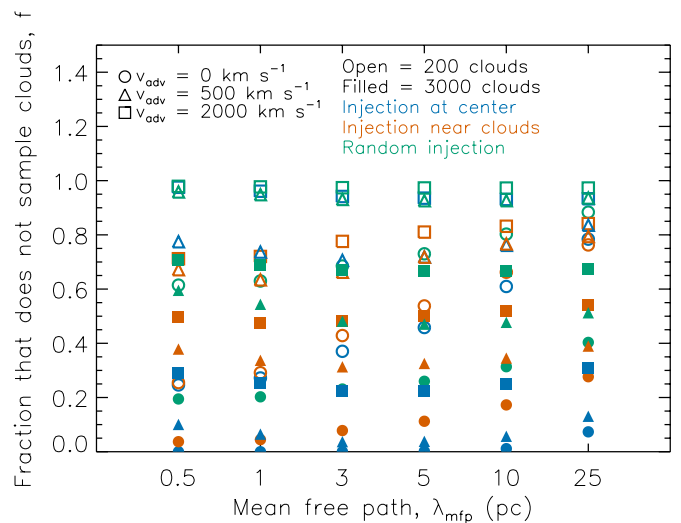


**Figure 5.** Fraction of cosmic rays  $f$  that escape the starburst region without sampling molecular clouds as a function of  $\lambda_{\text{mfp}}$ . Though the cosmic rays approximately sample the mean density of the ISM over much of parameter space, they clearly undergo a diverse range of sampling behaviors, from near complete sampling of clouds ( $f \sim 2 \times 10^{-5}$ ) to near absence of sampling ( $f \sim 0.98$ ). These fractions are determined from single  $N_p = 10^6$  particle runs, and will change slightly for different distributions of molecular clouds and cosmic ray injection sites. (A color version of this figure is available in the online journal.)

the cosmic ray calorimeter model, these two broad sampling behaviors can be considered comparable. However, if large numbers of cosmic rays escape from the starburst region without losing energy to collisional processes in the molecular medium, this may have important implications for the galactic environment. It has been shown that when the cosmic rays are self-confined, meaning that they generate the waves that trap them, they may contribute to driving a galactic wind (Breitschwerdt et al. 1991; Everett et al. 2008). Thus, we may be more likely to observe a galactic wind under conditions for which cosmic rays are able to travel through the hot medium to escape the starburst region without undergoing energy losses in molecular clouds.

## 4. DISCUSSION AND APPLICATIONS

### 4.1. Comparison to a “Back of the Envelope” Model

We now discuss our Monte Carlo simulations in the context of a simple, “back of the envelope” model of cosmic ray sampling of a clumpy ISM. We refer to the model in Section 4.1 of Yoa-Hull et al. (2013) adapted to account for diffusive cosmic ray propagation. This model suggests that cosmic rays will sample the mean density of the ISM if two general conditions are met. First, the magnetic field lines along which they propagate must pass through a representative sample of the varied components of the ISM. Second, they must be able to travel along or diffuse across field lines to encounter these components before they are advected from the region. To determine whether these conditions are met, we compare the timescale  $\tau_{\text{diff}}$  for cosmic rays to diffuse between clouds to the timescale  $\tau_{\text{adv}}$  for them to be advected from the region. We define the former as

$$\tau_{\text{diff}} = \frac{l_c^2}{v_A \lambda_{\text{mfp}}}, \quad (4)$$

where  $l_c$  is the mean distance between clouds and the factor of  $l_c/\lambda_{\text{mfp}}$  accounts for cosmic ray diffusion with a mean free path

$\lambda_{\text{mfp}} < l_c$ .  $l_c$  can be approximated as  $l_c \sim R/N_c^{1/3}$ , where  $R$  is the radius of the starburst region. We take  $l_c$  to be the mean minimum distance that cosmic rays must travel to reach a cloud assuming that there is no spatial correlation between clouds and cosmic ray injection sites. For this reason, this model is applicable only to cosmic rays traveling along sufficiently tangled magnetic field lines ( $\lambda_{\text{mfp}} < l_c$ ) and to cosmic rays that have been injected either centrally or randomly in the starburst region.

We define the condition under which cosmic rays will encounter molecular clouds to be

$$\frac{\tau_{\text{adv}}}{\tau_{\text{diff}}} \sim 2 \frac{v_A}{v_{\text{adv}}} \frac{\lambda_{\text{mfp}}}{R} N_c^{2/3} > 1, \quad (5)$$

where  $\tau_{\text{adv}} = 2R/v_{\text{adv}}$  is the advection timescale for cosmic rays that experience a mean advecting wind speed of  $\sim v_{\text{adv}}/2$ . Taking  $v_A = 960 \text{ km s}^{-1}$ ,  $v_{\text{adv}} = 500 \text{ km s}^{-1}$ , and  $R = 100 \text{ pc}$ , we arrive at a relationship between  $N_c$  and  $\lambda_{\text{mfp}}$  that predicts whether or not cosmic rays are able to encounter clouds before being advected from the starburst region:

$$N_c > \left( \frac{1}{(0.04 \text{ pc}^{-1}) \lambda_{\text{mfp}}} \right)^{3/2}. \quad (6)$$

We now compare this prediction with the results of our Monte Carlo simulations. Considering broadly the predictions of Equation (6) for central or random cosmic ray injection,  $v_{\text{adv}} = 500 \text{ km s}^{-1}$ , and  $\lambda_{\text{mfp}} < l_c$ , this prediction suggests that for all but the shortest  $\lambda_{\text{mfp}}$ , cosmic rays should encounter dense gas for both  $N_c = 200$  and 3000 clouds. For central injection, there is very good agreement between this prediction and our simulation results, as our  $\alpha$  values are indeed close to unity. For random injection, however, there is only very broad agreement, as  $\alpha$  is instead close to  $\sim 0.6$ . This discrepancy is not surprising for the case of random injection, as our simple model does not account for the effective decrease in the advection timescale for particles injected considerably closer than  $R = 100 \text{ pc}$  to the edge of the region.

Additionally, for  $\lambda_{\text{mfp}} = 0.5 \text{ pc}$ , Equation (6) suggests that we require  $N_c \gtrsim 350$  clouds for the cosmic rays to encounter dense gas. For central cosmic ray injection, however, we find from our simulations that the cosmic rays do indeed interact with dense gas for both  $N_c = 200$  and 3000 clouds. For random injection, we again find that the value of  $\alpha$  is relatively insensitive to cloud number. This discrepancy is due to our simple model's inability to account for the effect of increasing cloud density with decreasing cloud number. In our simulations, we find that despite fewer cosmic rays sampling clouds in the limit of small cloud number, we still observe emissivities comparable to those found for larger cloud numbers due to the increase in cloud density.

Thus, our simple model is useful for broadly considering constraints on the conditions for cosmic ray sampling of molecular clouds. However, this model solely suggests whether or not cosmic rays encounter dense gas. We have seen that the observed emissivity is dependent not only on getting cosmic rays to the gas, but on additional properties such as the gas density as well. Thus, for accurately predicting observed emissivities, our full Monte Carlo simulations are required to account for all relevant subtleties.

#### 4.2. Implications for Starburst Calorimeter Models

The starburst calorimeter model suggests that there is a direct relationship between the energy imparted to cosmic rays by

supernovae and the energy lost by cosmic rays within the starburst region. Thus, there is a relationship between the supernova rate, and therefore the SFR, and observable emission in the radio (cosmic ray electrons) and  $\gamma$ -ray (cosmic ray protons) regimes. Here, we evaluate the extent to which our simulated starburst region behaves as a cosmic ray calorimeter under a range of physical conditions by comparing the particles' confinement timescales  $\tau_C$  to their energy loss timescales  $\tau_E$ . Note that as starburst galaxies with properties like those of M82 are well established to be effective cosmic ray electron calorimeters (e.g., Yoast-Hull et al. 2013), we will consider only cosmic ray protons for the remainder of our analysis.

The cosmic ray transport equation gives rise to the functional form of  $\tau_E$  (e.g., Yoast-Hull et al. 2013) and is given by (Longair 2011)

$$\frac{\partial N(E, t)}{\partial t} = -\frac{\partial}{\partial E} \left[ \frac{dE}{dt} N(E, t) \right] + Q(E, t) - \frac{N(E, t)}{\tau_C}. \quad (7)$$

Here,  $N(E, t)dE$  is the cosmic ray number density at time  $t$  with energies between  $E$  and  $E + dE$ ,  $dE/dt$  is the rate at which radiative and collisional losses decrease a particle's energy, and  $Q(E, t)dE$  is the rate at which particles are injected per unit volume with energies between  $E$  and  $E + dE$ . Here,  $\tau_C$  accounts for both diffusive and advective losses and is assumed to be independent of energy. We may assume that  $Q(E)$  and  $N(E)$  are of the form  $Q(E) = AE^{-\gamma}$  and  $N(E) \approx Q(E)\tau(E)$ , where  $\tau(E)^{-1} \equiv \tau_C^{-1} + \tau_E^{-1}$  is the total energy loss rate. For the steady state, the energy loss rate  $\tau_E$  is then found to be

$$\tau_E \equiv -\frac{E}{dE/dt}. \quad (8)$$

The energy loss rates for cosmic ray protons are due primarily to ionization and pion production, the latter of which is dominant above  $\sim 1 \text{ GeV}$  (Schlickeiser 2002). Note that we do not account for the (negligible) contribution from Coulomb effects. The energy loss rates from both ionization and pion production are directly proportional to the average density sampled by the particles, defined as the mean density of the ISM modified by a multiplicative factor of  $\alpha$ ,  $\langle n_p \rangle = \alpha \langle n_{\text{SB}} \rangle$ . We define the confinement timescale  $\tau_C$  for a given  $v_{\text{adv}}$ ,  $\lambda_{\text{mfp}}$ , and cosmic ray injection mechanism as the median time that  $N_p = 10^6$  particles take to escape from the starburst region. We calculate the ratio of the confinement to energy loss timescales  $\tau_C/\tau_E$  and seek physical conditions where the calorimeter model fails to hold ( $\tau_C/\tau_E \ll 1$ ).

In Figure 6, we show  $\tau_C/\tau_E$  for  $E = 1 \text{ GeV}$  and  $E = 1 \text{ TeV}$  protons over the full parameter space considered. At a given energy, the value of  $\tau_C/\tau_E$  ranges over more than three orders of magnitude and is strongly dependent on  $v_{\text{adv}}$ ,  $\lambda_{\text{mfp}}$ , and the cosmic ray injection mechanism. For the lowest energy protons ( $E \sim 0.1 \text{ GeV}$ ),  $\tau_C/\tau_E \gtrsim 1$  for all parameters considered, and the starburst region is an effective proton calorimeter. At moderate proton energies ( $E \sim 1 \text{ GeV}$ ), however,  $\tau_C/\tau_E$  only exceeds unity for all  $\lambda_{\text{mfp}}$  in the absence of a galactic wind. Additionally,  $\tau_C/\tau_E$  does not exceed unity for the longest  $\lambda_{\text{mfp}}$  for any parameters considered. At higher energies ( $E \sim 1 \text{ TeV}$ ),  $\tau_C/\tau_E$  again exceeds unity in all cases except that of large  $N_c$ , high  $v_{\text{adv}}$ , and injection throughout the region. Thus, for moderate to high proton energies, our simulated starburst region can only be deemed a partial proton calorimeter without further knowledge of the physical conditions in the region. Note that

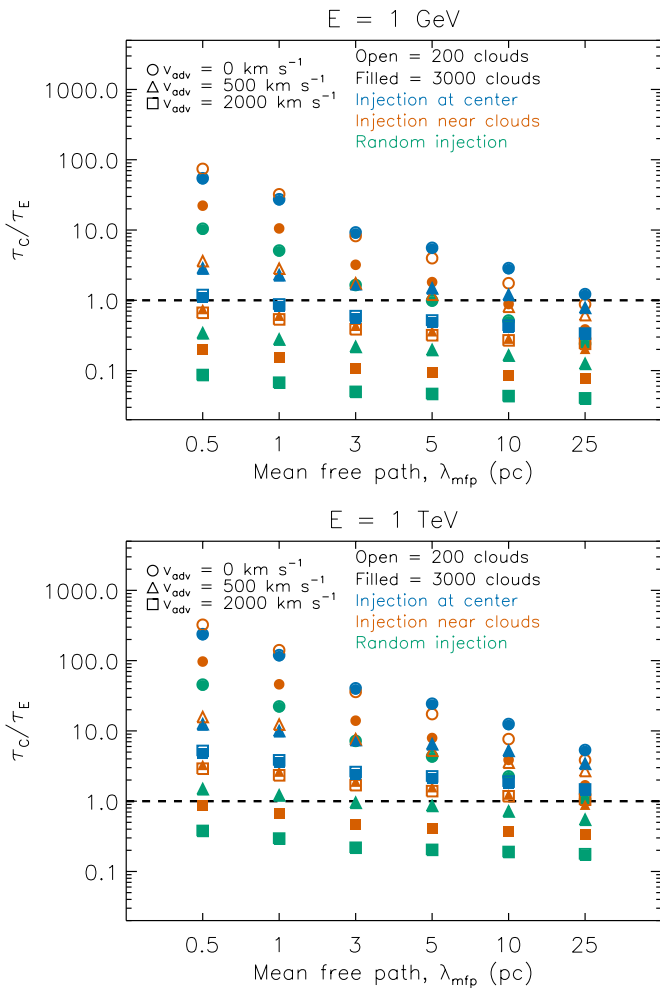


**Figure 6.** To assess whether our simulated starburst region is an effective cosmic ray proton calorimeter, we examine the ratio of the confinement timescale  $\tau_C$  to the energy loss timescale  $\tau_E$ . Here, we consider  $\tau_C/\tau_E$  for  $E = 1$  GeV and  $E = 1$  TeV protons for a range of conditions on  $N_c$ ,  $\lambda_{\text{mfp}}$ ,  $v_{\text{adv}}$ , and the cosmic ray injection mechanism. Although the starburst region is an effective proton calorimeter at low energies ( $\tau_C/\tau_E > 1$ ,  $E \sim 0.1$  GeV), it may be at best a partial proton calorimeter for the energies considered here, where  $\tau_C/\tau_E \lesssim 1$  over non-trivial portions of parameter space.

(A color version of this figure is available in the online journal.)

the starburst region would be calorimetric over larger portions of parameter space if we had made a more generous estimate of the molecular gas mass contained within the region.

#### 4.3. The Spectrum of a Cosmic Ray Burst

We conclude by constructing the spectrum of a cosmic ray burst from a single supernova explosion and evaluating how the time evolution of the spectrum is affected by the density sampled by the particles. Although the steady state solution is generally preferred for the cosmic ray populations of starburst galaxies, the behavior of a burst of cosmic rays may inform our understanding of how smaller scale cosmic ray populations evolve over short timescales. Here, we again consider only cosmic ray protons, as only a small minority of a supernova's energy is believed to be imparted to cosmic ray electrons (Blandford & Eichler 1987).

To construct the spectrum of a burst of cosmic rays, we begin by dropping both the source and the advection terms from the cosmic ray transport equation; the advection term will be added

later. Thus, we have

$$\frac{\partial N(E, t)}{\partial t} = \frac{\partial}{\partial E} [b(E)N(E, t)], \quad (9)$$

where we define the energy loss rate to be

$$b(E) = -\frac{dE}{dt}. \quad (10)$$

For initial condition  $N(E, 0) = N_o(E)$ , one can show that  $N(E, t)$  takes the form

$$N(E, t) = N_o(E_o(E, t)) \frac{b(E_o)}{b(E)}, \quad (11)$$

where  $E_o(E, t)$  is the energy at time  $t = 0$  of a particle with energy  $E$  at time  $t$ .

We now restore the advection term to the cosmic ray transport equation

$$\frac{\partial N(E, t)}{\partial t} = \frac{\partial}{\partial E} [b(E)N(E, t)] - \frac{N(E, t)}{\tau_C}. \quad (12)$$

We consider the case where  $N(E, t)$  assumes the form  $N(E, t) = f(E, t)e^{-t/\tau_C}$ . By substituting this expression into the transport equation with advective losses added, we discover that  $f(E, t)$  is a solution of this equation when advective losses are neglected. Thus, we obtain an expression for  $N(E, t)$  accounting for advective losses by multiplying our previous expression for  $N(E, t)$  by a factor of  $e^{-t/\tau_C}$ . Additionally, we assume that the initial injected spectrum is a power law  $N_o(E) = AE^{-\gamma}$  with spectral index  $\gamma \gtrsim 2$ . Therefore, the spectrum of a burst of cosmic rays has the functional form

$$N(E, t) = A(E_o(E, t))^{-\gamma} e^{-t/\tau_C} \frac{b(E_o)}{b(E)}. \quad (13)$$

To find the initial energy  $E_o$  given the energy  $E$  at time  $t$ , we solve for the value of  $E_o$  that satisfies

$$t = \int_E^{E_o} \frac{dE'}{b(E')}. \quad (14)$$

This is done by selecting a value for  $E_o$ , numerically integrating backward, and evaluating the consistency of the resulting  $t'$  with the desired time  $t$ .

Finally, we determine the value of  $A$  in order to satisfy

$$\int_{E_{\text{min}}}^{E_{\text{max}}} N_o(E)E dE = \frac{E_{\text{SN}}\eta}{V_{\text{SB}}}, \quad (15)$$

where  $E_{\text{SN}}$  is the energy released by a supernova explosion,  $\eta$  is the fraction of a supernova's energy transferred to cosmic rays, and  $V_{\text{SB}}$  is the volume of the starburst region. Therefore,  $A$  has the functional form:

$$A = \frac{(\gamma - 2) E_{\text{SN}}\eta}{E_{\text{min}}^{-\gamma+2} V_{\text{SB}}}, \quad (16)$$

where we take  $\gamma = 2.1$ ,  $E_{\text{min}} = 0.1$  GeV,  $E_{\text{SN}} = 10^{51}$  erg,  $\eta = 0.1$ , and  $V_{\text{SB}} \sim 10^{62}$  cm<sup>3</sup>. Note that we take the cosmic ray acceleration timescale in a supernova shock to be  $\tau_{\text{accel}} \lesssim 10^4$  yr  $\ll \tau_C$ , and thus  $\tau_{\text{accel}}$  can be taken to be effectively instantaneous.

The time evolution of the spectrum is shown in the upper panel of Figure 7 for  $\alpha = 1$  and  $\tau_C = 10^6$  yr. This choice of  $\alpha$  and  $\tau_C$

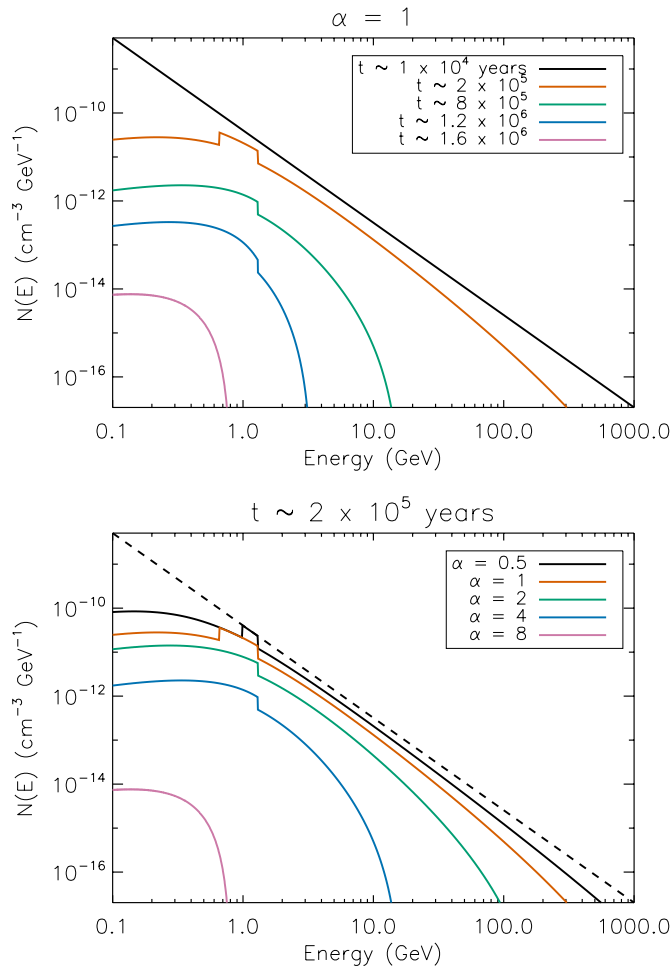


**Figure 7.** In the upper panel, we show the time evolution of the spectrum of a burst of cosmic ray protons from a single supernova explosion under the physical conditions of M82. Here, we take  $\alpha = 1$  and  $\tau_C = 10^6$  yr, values consistent with much of the parameter space considered. Other confinement times can be easily accounted for by appropriately adjusting the factor of  $e^{-t/\tau_C}$  in Equation (13). The rapid evolution of the spectrum with time suggests that cosmic ray bursts are short lived in these environments. In the lower panel, we show the spectrum of a cosmic ray burst at time  $t \sim \tau_{\text{accel}}$  (dashed line) as well as at  $t \sim 2 \times 10^5$  yr (solid lines) for a range of values of  $\alpha$ . It is clear that cosmic ray bursts that sample densities greater than the mean density of the ISM by a factor of a few have dramatically shortened lifetimes.

(A color version of this figure is available in the online journal.)

is consistent with much of the parameter space considered. As in Section 4.2, the energy loss rates for cosmic ray protons are calculated according to Schlickeiser (2002). It is evident that the spectrum evolves rapidly with time; on timescales comparable to the confinement time, the number density decreases by several orders of magnitude at all energies. This decline is most dramatic at high energies ( $E \gtrsim 10$  GeV), where the spectrum steepens sharply by  $t \sim 10^6$  yr due to extreme energy loss rates as well as the initial lack of high-energy particles.

In the lower panel of Figure 7, we show the spectrum at time  $t \sim 2 \times 10^5$  yr for a range of densities sampled. It is clear that increasing the value of  $\alpha$  by a factor of a few rapidly decreases the lifetime of the particle population. For example, by comparing the top and bottom panels of Figure 7, we see that the spectrum of a cosmic ray burst with  $\alpha = 1$  that has evolved for  $t \sim 1.6 \times 10^6$  yr is identical to the spectrum of a burst with  $\alpha = 8$  that has evolved for only  $t \sim 2 \times 10^5$  yr.

Overall, the spectrum of a burst of cosmic rays evolves rapidly under the physical conditions of a starburst galaxy like

M82, and thus the cosmic ray population produced by a single supernova explosion under these conditions is a short-lived phenomenon. However, a conservative estimate of the supernova rate in M82 is  $\sim 0.07 \text{ yr}^{-1}$  (Fenech et al. 2008), and thus we can expect that a supernova explosion will occur in M82 every  $\sim 15$  yr. The evolved cosmic ray spectra shown in Figure 7 will therefore never be made manifest, and instead will be regularly replenished by newly injected particles. However, in other star-forming environments where the supernova rate may be very low, such as extreme dwarf galaxies or OB associations, these spectra may indeed be manifested due to a lack of replenishing particles.

## 5. CONCLUSIONS

In the interest of understanding how cosmic rays sample the clumpy ISM in a starburst environment, we have undertaken Monte Carlo simulations of cosmic ray sampling of molecular clouds under the physical conditions of the archetypal starburst galaxy M82. Here, we briefly review the results of our study.

1. Cosmic rays sample roughly the mean density of the ISM ( $\alpha \sim 1$ ) for a wide range of assumptions about the number of molecular clouds, the galactic wind speed, the extent to which the magnetic field is tangled, and the cosmic ray injection mechanism. A value of  $\alpha \sim 1$  is consistent with models of the observed  $\gamma$ -ray spectrum of M82 (Yoast-Hull et al. 2013).
2. Cosmic rays sample densities a factor of a few higher than the mean density ( $2 \lesssim \alpha \lesssim 7.5$ ) in the case of a small number of dense molecular clouds, injection close to the clouds, and a highly tangled magnetic field.
3. The fraction of cosmic rays that escape from the starburst region without sampling molecular clouds ranges from  $10^{-5} \lesssim f \lesssim 0.98$  for physical conditions that yield  $\alpha \sim 1$ . This suggests that although the sampling behavior of the cosmic ray population as a whole is largely independent of the physical conditions, the behavior of individual particles is not.
4. Our simulated starburst region is at least a partial cosmic ray proton calorimeter, and appears to be a complete calorimeter at all proton energies for no galactic wind and short cosmic ray mean free path.
5. We construct the time-dependent spectrum of a burst of cosmic rays, and demonstrate that the spectrum evolves rapidly under the physical conditions of M82. However, these spectra are only made manifest in environments with very low supernova rates ( $< 10^{-5} \text{ yr}^{-1}$ ) where the spectra are not continuously replenished with energetic particles.

Though we have illustrated several applications here, cosmic ray sampling of a clumpy ISM may be applied to a wide range of science goals seeking to understand the relationship between the state of the multi-phase ISM, the star formation processes, and the cosmic ray populations of starburst galaxies.

We gratefully acknowledge the support of NSF AST-0907837 and NSF PHY-0821899 (to the Center for Magnetic Self-Organization in Laboratory and Astrophysical Plasmas). We thank Benjamin Brown, Sebastian Heinz, Dan McCammon, and Joshua Wiener for helpful discussions, as well as Masataka Okabe and Kei Ito for supplying the colorblind-friendly color palette used in this paper (see <http://jfly.iam.u-tokyo.ac.jp/color/index.html>). This work has made use of NASA's Astrophysics Data System.

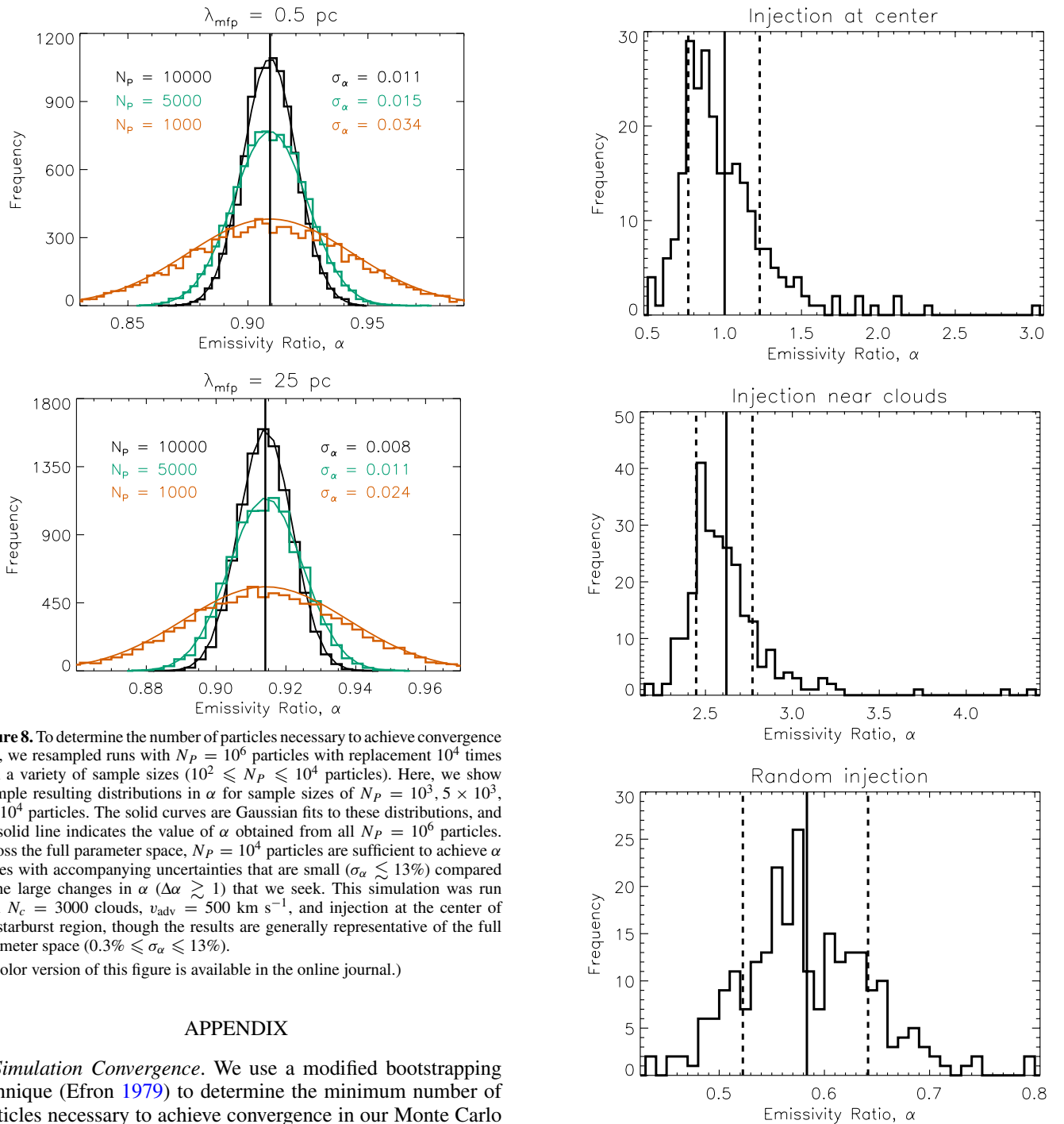


**Figure 8.** To determine the number of particles necessary to achieve convergence in  $\alpha$ , we resampled runs with  $N_p = 10^6$  particles with replacement  $10^4$  times with a variety of sample sizes ( $10^2 \leq N_p \leq 10^4$  particles). Here, we show example resulting distributions in  $\alpha$  for sample sizes of  $N_p = 10^3$ ,  $5 \times 10^3$ , and  $10^4$  particles. The solid curves are Gaussian fits to these distributions, and the solid line indicates the value of  $\alpha$  obtained from all  $N_p = 10^6$  particles. Across the full parameter space,  $N_p = 10^4$  particles are sufficient to achieve  $\alpha$  values with accompanying uncertainties that are small ( $\sigma_\alpha \lesssim 13\%$ ) compared to the large changes in  $\alpha$  ( $\Delta\alpha \gtrsim 1$ ) that we seek. This simulation was run with  $N_c = 3000$  clouds,  $v_{\text{adv}} = 500 \text{ km s}^{-1}$ , and injection at the center of the starburst region, though the results are generally representative of the full parameter space ( $0.3\% \leq \sigma_\alpha \leq 13\%$ ).

(A color version of this figure is available in the online journal.)

## APPENDIX

*Simulation Convergence.* We use a modified bootstrapping technique (Efron 1979) to determine the minimum number of particles necessary to achieve convergence in our Monte Carlo simulations. For each cosmic ray mean free path, injection mechanism, and parameter extrema (i.e.,  $N_c = 200$  and 3000 clouds,  $v_{\text{adv}} = 0, 500$ , and  $2000 \text{ km s}^{-1}$ ), we resampled an  $N_p = 10^6$  particle run with replacement  $10^4$  times for a range of sample sizes ( $10^2 \leq N_p \leq 10^4$ ). We calculated a new value of  $\alpha$  for each selected sample and fit the resulting distributions in  $\alpha$  with Gaussian profiles to determine their standard deviations. As we are primarily interested in areas of parameter space where  $\alpha$  departs significantly from unity, our purposes are easily served by uncertainties in  $\alpha$  on the order of  $\sim 10\%$ . In Figure 8, we show an example of the resulting distributions in  $\alpha$  with a range of sample sizes.

For a sample size of  $N_p = 10^4$  particles, the spreads of the resulting Gaussian distributions ( $\sigma_\alpha$ ) range from  $\sim 0.33\%$  (for  $N_c = 3000$  clouds,  $v_{\text{adv}} = 0 \text{ km s}^{-1}$ , and central injection)

**Figure 9.** Sample emissivity distributions for each injection mechanism used to obtain the value of  $\alpha$  and the corresponding uncertainty associated with the changes in the cloud and injection site distributions from run to run. The solid line indicates the mean of the distribution, and the dashed lines the 68% confidence intervals. While random cosmic ray injection results in fairly Gaussian distributions, it is clear that injection at the center and near clouds result in distributions that are non-Gaussian with sparsely populated tails at high emissivities. These simulations have  $N_c = 200$  clouds,  $\lambda_{\text{mfp}} = 5 \text{ pc}$ , and  $v_{\text{adv}} = 500 \text{ km s}^{-1}$ . Note that the apparent asymmetry in the area enclosed by the 68% confidence intervals in the top and middle panels is due to the choice of binning.

to  $\sim 13\%$  (for  $N_c = 200$  clouds,  $v_{\text{adv}} = 2000 \text{ km s}^{-1}$ , and random injection). Decreasing the sample size to  $N_p = 5000$  particles increases  $\sigma_\alpha$  by  $\sim 40\%$ , and to  $N_p = 1000$  particles increases  $\sigma_\alpha$  by more than 200%. Additionally, the case of

$N_c = 200$  clouds and injection randomly throughout the region results in skewed distributions with significant tails toward high emissivities for  $N_p = 1000$  and 5000 particles, although the skew is negligible for  $N_p = 10^4$  particles. Thus, we select  $N_p = 10^4$  particles as the number of particles necessary to achieve convergence, because this sample size allows  $\sigma_\alpha$  to remain below or comparable to  $\sim 10\%$  and our resampled distributions to remain Gaussian across the full parameter space.

*Error Estimation.* The generally dominant source of uncertainty in  $\alpha$  for a given choice of  $N_c$ ,  $v_{\text{adv}}$ ,  $\lambda_{\text{mfp}}$ , and cosmic ray injection mechanism is associated with the changes in the molecular cloud and injection site distributions from run to run. To quantify this uncertainty, we ran repeated runs varying only the cloud distribution (for central injection) or the cloud and injection site distributions (for the other injection methods) until sufficiently sampled emissivity distributions were obtained (i.e.,  $\sim 250$  runs). As shown in Figure 9, the shape and spread of the emissivity distributions are dependent on the cosmic ray injection mechanism. Random injection results in fairly Gaussian distributions with modest spreads ( $\sigma_\alpha \sim 0.01\text{--}0.1$ ), while the other injection methods result in slightly to severely skewed distributions with sparsely populated tails at high emissivities. These latter injection mechanisms also result in significant spreads ( $\sigma_\alpha \sim 0.03\text{--}1.0$ , injection at center;  $\sigma_\alpha \sim 0.05\text{--}2.5$ , injection near clouds). The mean emissivities and 68% confidence intervals obtained from these distributions are the emissivities and error bars reported in this work.

## REFERENCES

- Abdo, A. A., Ackermann, M., Ajello, M., et al. 2010, *ApJ*, **718**, 348  
 Abdo, A. A., Ackermann, M., Ajello, M., et al. 2011, *ApJ*, **734**, 28  
 Aharonian, F., Akhperjanian, A. G., Barres de Almeida, U., et al. 2008a, *A&A*, **490**, 685  
 Aharonian, F., Akhperjanian, A. G., Bazer-Bachi, A. R., et al. 2008b, *A&A*, **481**, 401  
 Ajello, M., Allafort, A., Baldini, L., et al. 2012, *ApJ*, **744**, 80  
 Bell, A. R. 1978, *MNRAS*, **182**, 147  
 Blandford, R., & Eichler, D. 1987, *PhR*, **154**, 1  
 Blandford, R. D., & Ostriker, J. P. 1978, *ApJL*, **221**, L29  
 Blitz, L. 1993, in *Protostars and Planets III*, ed. E. H. Levy & J. I. Lunine (Tucson, AZ: Univ. Arizona Press), 125  
 Breitschwerdt, D., McKenzie, J. F., & Voelk, H. J. 1991, *A&A*, **245**, 79  
 Chevalier, R. A., & Clegg, A. W. 1985, *Natur*, **317**, 44  
 de Cea del Pozo, E., Torres, D. F., & Rodriguez Marrero, A. Y. 2009, *ApJ*, **698**, 1054  
 Efron, B. 1979, *AnSta*, **7**, 1  
 Everett, J. E., Zweibel, E. G., Benjamin, R. A., et al. 2008, *ApJ*, **674**, 258  
 Fenech, D., Beswick, R., Muxlow, T. W. B., Pedlar, A., & Argo, M. K. 2010, *MNRAS*, **408**, 607  
 Fenech, D. M., Muxlow, T. W. B., Beswick, R. J., Pedlar, A., & Argo, M. K. 2008, *MNRAS*, **391**, 1384  
 Fermi, E. 1949, *PhRv*, **75**, 1169  
 Förster Schreiber, N. M., Sauvage, M., Charmandaris, V., et al. 2003, *A&A*, **399**, 833  
 Helou, G., Soifer, B. T., & Rowan-Robinson, M. 1985, *ApJL*, **298**, L7  
 Inoue, T., & Inutsuka, S. 2012, *ApJ*, **759**, 35  
 Kulsrud, R., & Pearce, W. P. 1969, *ApJ*, **156**, 445  
 Lacki, B. C., Thompson, T. A., Quataert, E., Loeb, A., & Waxman, E. 2011, *ApJ*, **734**, 107  
 Longair, M. S. 2011, *High Energy Astrophysics* (3rd ed.; Cambridge: Cambridge Univ. Press)  
 Naylor, B. J., Bradford, C. M., Aguirre, J. E., et al. 2010, *ApJ*, **722**, 668  
 Paglione, T. A. D., & Abrahams, R. D. 2012, *ApJ*, **755**, 106  
 Persic, M., Rephaeli, Y., & Arieli, Y. 2008, *A&A*, **486**, 143  
 Sakai, S., & Madore, B. F. 1999, *ApJ*, **526**, 599  
 Schleicher, D. R. G., & Beck, R. 2013, *A&A*, **556**, A142  
 Schlickeiser, R. 2002, *Cosmic Ray Astrophysics* (Berlin: Springer)  
 Shoppell, P. L., & Bland-Hawthorn, J. 1998, *ApJ*, **493**, 129  
 Strickland, D. K., & Heckman, T. M. 2009, *ApJ*, **697**, 2030  
 Thompson, T. A., Quataert, E., Waxman, E., Murray, N., & Martin, C. L. 2006, *ApJ*, **645**, 186  
 Voelk, H. J. 1989, *A&A*, **218**, 67  
 Westmoquette, M. S., Gallagher, J. S., Smith, L. J., et al. 2009, *ApJ*, **706**, 1571  
 Wild, W., Harris, A. I., Eckart, A., et al. 1992, *A&A*, **265**, 447  
 Yoast-Hull, T. M., Everett, J. E., Gallagher, J. S., III., & Zweibel, E. G. 2013, *ApJ*, **768**, 53